J Neurophysiol 89: 3143–3154, 2003.
First published February 26, 2003; 10.1152/jn.00046.2003.

Coincidence Detection in Pyramidal Neurons Is Tuned by Their Dendritic Branching Pattern

Andreas T. Schaefer, Matthew E. Larkum, Bert Sakmann, and Arnd Roth
Abteilung Zellphysiologie, Max-Planck-Institut für medizinische Forschung, D-69120 Heidelberg, Germany

Submitted 16 January 2003; accepted in final form 17 February 2003

Schaefer, Andreas T., Matthew E. Larkum, Bert Sakmann, and Arnd Roth. Coincidence detection in pyramidal neurons is tuned by their dendritic branching pattern. *J Neurophysiol* 89: 3143–3154, 2003. First published February 26, 2003; 10.1152/jn.00046.2003. Neurons display a variety of complex dendritic morphologies even within the same class. We examined the relationship between dendritic arborization and the coupling between somatic and dendritic action potential (AP) initiation sites in layer 5 (L5) neocortical pyramidal neurons. Coupling was defined as the relative reduction in threshold for initiation of a dendritic calcium AP due to a coincident back-propagating AP. Simulations based on reconstructions of biocytin-filled cells showed that addition of oblique branches of the main apical dendrite in close proximity to the soma ($d < 140$ μm) increases the coupling between the apical and axosomatic AP initiation zones, whereas incorporation of distal branches decreases coupling. Experimental studies on L5 pyramids in acute brain slices revealed a highly significant ($n = 28$, $r = 0.63$, $P < 0.0005$) correlation: increasing the fraction of proximal oblique dendrites ($d < 140$ μm), e.g., from 30 to 60% resulted on average in an increase of the coupling from approximately 35% to almost 60%. We conclude that variation in dendritic arborization may be a key determinant of variability in coupling (49 ± 17%; range 19–83%; $n = 37$) and is likely to outweigh the contribution made by variations in active membrane properties. Thus coincidence detection of inputs arriving from different cortical layers is strongly regulated by differences in dendritic arborization.

INTRODUCTION

Is morphological variation a bug that arises from intrinsic biological variability or a feature that extends the computational capabilities of a neuron? Since the studies of Cajal (Ramón y Cajal 2001), morphology has been one of the main criteria for defining classes and subclasses of neurons (Connors and Gutnick 1990; Gupta et al. 2000; Kim and Connors 1993). The diversity of morphologies also raises questions about its possible functional implications. Clearly, dendritic as well as axonal branching patterns determine the connectivity between neurons in the network. However, does morphological variation *directly* influence the rules of synaptic integration in single neurons? It is well established (Segev et al. 1995) that the cable properties of dendrites determine the spread of subthreshold postsynaptic potentials. Recent modeling studies showed that even differences in active properties between cells, such as intrinsic firing pattern (Mainen and Sejnowski 1996) or action potential (AP) propagation (Vetter et al. 2001), could in principle simply result from differences in the morphology of dendritic arbors.

So far, most studies on the role of morphology have compared different cell classes (Kim and Connors 1993; Mainen and Sejnowski 1996; Vetter et al. 2001). In these cases, in addition to the morphological differences, there are also significant differences in the distribution and types of ion channels (Häusser et al. 2000; Serodio and Rudy 1998; Talley et al. 1999). This makes it particularly difficult to determine the relative influence of morphology on the properties of different cell types.

Here we focused on variations of the dendritic branching pattern *within* one class of cells, thick tufted neocortical layer 5 (L5) pyramidal neurons. This cell type is one of the largest found in the mammalian cortex. Its prominent apical dendrite extends vertically ≤1.3 mm from the soma and gives rise to a tuft of dendritic branches in layer 1 and oblique dendrites spreading horizontally in layers 2/3 and 4. The detailed branching pattern varies considerably between individual cells. L5 pyramidal cells also display ≥2 major types of regenerative events: First, sodium based APs (Na^+-APs) are initiated close to the soma and propagate back into the dendritic arbor [back-propagating AP (bAP); Stuart and Sakmann 1994]; second, long-lasting, mainly Ca^{2+} mediated depolarizations (Ca^{2+}-APs) are initiated predominantly in the distal regions of the apical dendrite (Helmchen et al. 1999; Schiller et al. 1995, 1997) and can be evoked by strong distal synaptic input. It was recently shown that a bAP can lower the threshold for initiation of a Ca^{2+}-AP, thus enabling L5 pyramidal neurons to couple synaptic inputs from different cortical layers if they coincide within a short time window [Fig. 1; backpropagation activated Ca^{2+} spike firing (BAC firing); Larkum et al. 1999a,b, 2001].

We show, by combining simulations and experiments, that the detailed geometry of proximal and distal oblique dendrites originating from the main apical dendrite determines the degree of coupling between the proximal and distal AP initiation zones. We found that morphological differences between neurons of the same type contribute in a specific way to the observed functional diversity, regardless of cell-to-cell variability in ion channel distribution. Structural plasticity (Cline 2001; Maletic-Savatic et al. 1999; Poirazi and Mel 2001) of the dendritic arbor could be one way to regulate the response properties of L5 pyramidal neurons to coincident synaptic inputs arriving at different cortical layers.

Address for reprint requests: A. T. Schaefer, Abteilung Zellphysiologie, Max-Planck-Institut für medizinische Forschung, Jahnstraβe 29, D-69120 Heidelberg, Germany (E-mail: schaefer@mpimf-heidelberg.mpg.de).

The costs of publication of this article were defrayed in part by the payment of page charges. The article must therefore be hereby marked "*advertisement*" in accordance with 18 U.S.C. Section 1734 solely to indicate this fact.

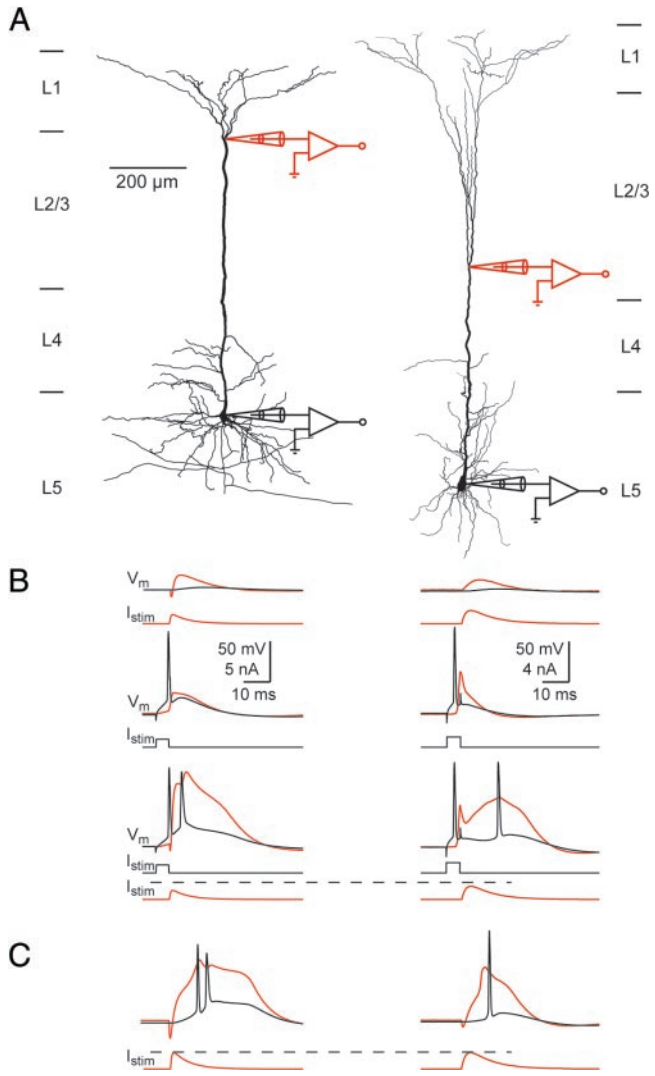

FIG. 1. Variability of morphology and experimentally measured backpropagation activated Ca^{2+} spike firing (BAC firing) in 2 layer 5 (L5) pyramidal neurons. *A*: reconstructions of 2 L5 pyramidal neurons with the locations of recording pipettes (soma, black; dendrite, red) depicted schematically. *B*: BAC firing. Distal current injection of 1.1 (*left*) and 1.3 nA (*right*) in the shape of an excitatory postsynaptic potential (EPSP; I_{stim}, red) evoked only weak somatic (black) depolarization (*top*). Threshold current injection (5 ms) into the soma (black) produced an action potential (AP) that propagated back into the apical dendritic arbor [backpropagating action potential (bAP); red, *middle*]. Combination of somatic and dendritic current injection generates several somatic APs and a dendritic Ca^{2+}-AP (BAC firing, *bottom*). Dashed line indicates the current threshold for a dendritic Ca^{2+}-AP alone. *C*: dendritic Ca^{2+}-AP was evoked by 2- (*left*) or 1.6-nA (*right*) current injection into the apical dendrite alone. Thus the bAP reduced the threshold for dendritic Ca^{2+}-APs by 0.9 nA (*left*, 45% coupling) or 0.3 nA (*right*, 19% coupling), respectively.

METHODS

Definitions of cell populations

Five populations of cells were used in this work.

ELECTROPHYSIOLOGICALLY STUDIED NEURONS (POPULATION 1). Dual and triple whole cell recordings were performed on single, identified pyramidal neurons in L5 in slices from somatosensory cortex of P28–P59 Wistar rats as described previously (Larkum et al. 1999b, 2001); there was no significant correlation between coupling and age (coupling changes by 5.8 ± 3.3% for each 10 postnatal days, Pearson correlation coefficient $r = 0.28$, $n = 37$, $P = 0.1$). Somatic current injection identified the cells recorded from as regular spiking pyramidal cells (Connors and Gutnick 1990; Kim and Connors 1993; Larkum et al. 1999b, 2001). Stable whole cell recordings with at least one somatic and one dendritic pipette (Fig. 1) were obtained from 37 L5 pyramidal cells so that the BAC firing threshold reduction could be measured. The dendritic electrode was located at 670 ± 18 μm (SE) from the soma (range, 443–890 μm; there was no correlation between recording distance and coupling; coupling increased by 1.8 ± 2.6% per 100 μm, $r = 0.12$, $n = 37$, $P > 0.4$).

SCHEMATICALLY RECONSTRUCTED NEURONS (POPULATION 2). For 28 of the 37 neurons from population 1, not necessarily the entire dendritic arbor, but at least the position of the origins of all oblique dendrites could be determined. Thus for this group, both detailed electrophysiological and sufficient morphological information were available to directly test the hypothesis that the position of oblique dendrites determines the degree of coupling between axosomatic and dendritic AP initiation sites (Figs. 8 and 9).

RECONSTRUCTED MODEL NEURONS (POPULATION 3). Pyramidal neurons in L5 were filled with biocytin during various electrophysiological recordings in acute brain slices (4 experiments from population 1). All slices were from the somatosensory cortex of P28–P59 Wistar rats. After recordings, slices were fixed by immersion in 4% paraformaldehyde in 0.1 M phosphate buffer. Tissue sections were processed with the avidin-biotin-peroxidase method to reveal cell morphology. Twenty-nine cells were recovered, and their dendritic morphology was reconstructed in detail with the aid of a computerized reconstruction system (Neurolucida, MicroBrightField, Colchester, VT) and converted to compartmental models in NEURON (Hines and Carnevale 1997) format using programs written in C. Simulations were performed using NEURON version 4.1.1 running on a Silicon Graphics Origin 2000 server. The time step was 25 μs, and the spatial compartment size did not exceed 20 μm. Axial resistance and membrane resistance were $R_i = 80$ Ωcm and $R_m = 30$ kΩcm^2, respectively, unless otherwise noted; the membrane capacitance was in general set to $C_m = 0.6$ μF/cm^2 (e.g., Major et al. 1994; Roth and Häusser 2001). Dendritic spines were accounted for by doubling membrane capacitance and conductances. Ion channels were incorporated into the membrane of each compartment according to the "active membrane model" as specified below [Figs. 2 and 3; the pictures in Fig. 2 are stills from a movie, which may be downloaded from our server (http://sun0.mpimf-heidelberg.mpg.de/~schaefer/BACFiring) and is also available as Supplementary Material at the *Journal of Neurophysiology* web site].[1]

SYNTHETIC MODEL NEURONS (POPULATION 4). As described in RESULTS, 32 synthetic morphologies were computer generated. The aim of the synthesis was to obtain an ensemble of synthetic model neurons that matched a given ensemble of reconstructed model neurons in both mean and SD of all parameters listed below as the "dendritic fingerprint." The variables required for the synthesis were drawn randomly from Gaussian distributions with the same mean and SD as the respective parameter distributions for the reconstructed model neurons. This resulted in a set of target morphological parameters that describe the individual morphology of a synthetic model neuron to be generated using the following algorithm: First, a number of basal dendrites, n_B, was drawn from the appropriate distribution. Second, single branches (1 apical dendrite and n_B basal dendrites) were synthesized: The parameters of the dendritic fingerprint for an individual neuron were again drawn independently from Gaussian distributions with the same mean and SD as given by the ensemble parameter sets (Figs. 4 and 5*D*). This resulted in a target connectivity describing the dendritic branching pattern for the individual neuron to be synthesized.

[1] The supplementary material (a movie file) for this article is available online at http://jn.physiology.org/cgi/content/full/89/6/3143/DC1

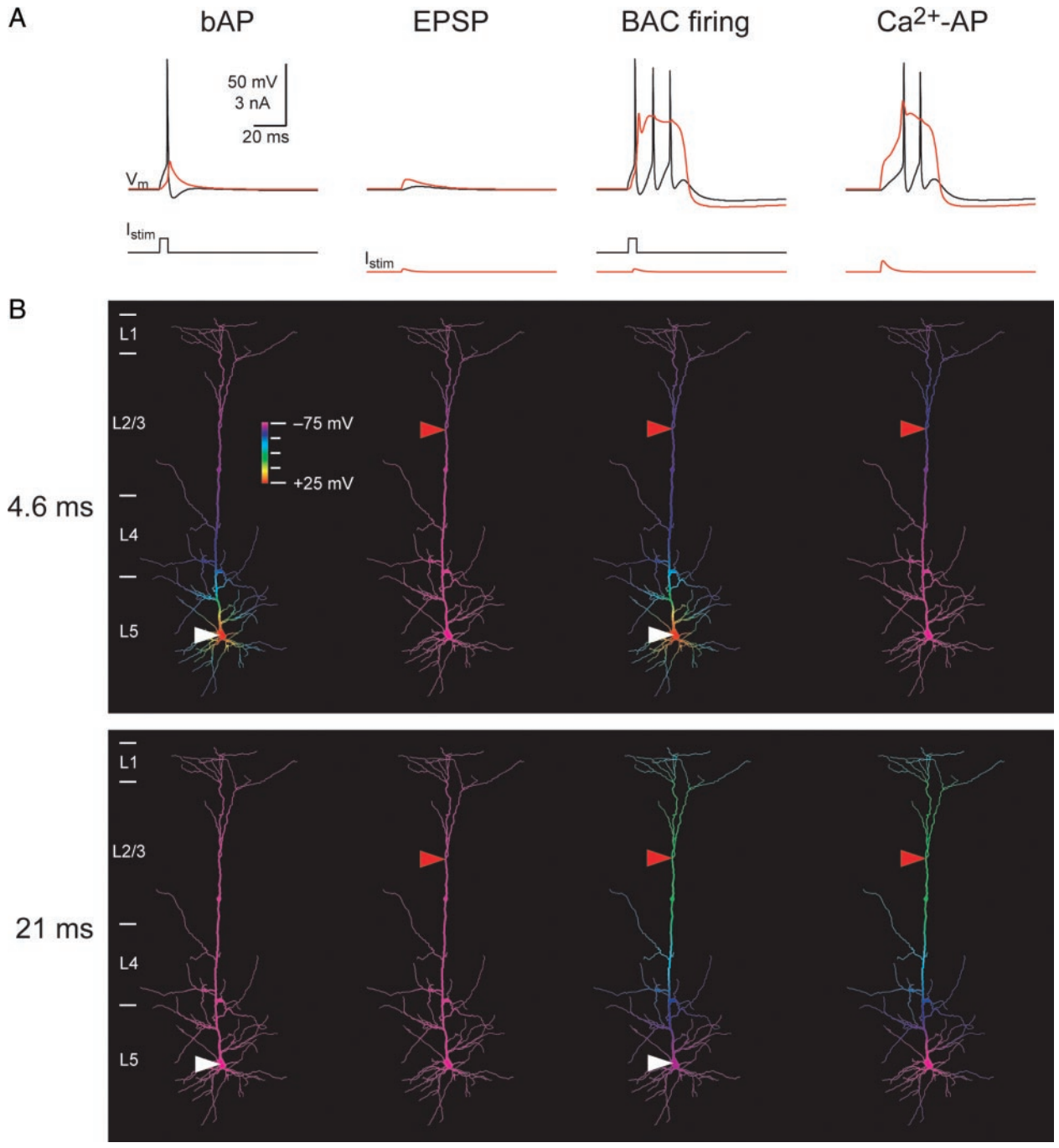

FIG. 2. Model of BAC firing in L5 pyramidal neurons. A model of channel density distributions and kinetics was constructed to reproduce BAC firing in reconstructed model neurons (METHODS). The electrical response of the reconstructed model neurons to dendritic and somatic current injection was investigated using the same protocols as in the experiment (Fig. 1). *A*: bAP: threshold somatic current injection evoked a bAP (I_{inj} = 1.9 nA). EPSP: distal EPSP-like current injection was adjusted to BAC firing threshold, which was 0.6 nA. Only a small somatic depolarization can be detected ($\Delta V \leq 2.5$ mV). BAC firing: pairing the bAP with the dendritic EPSP-like current injection resulted in a large and long-lasting dendritic depolarization. Ca^{2+}-AP: large distal EPSP-like current injection (1.7 nA) elicited a Ca^{2+}-AP. Thus the bAP reduced the threshold for dendritic Ca^{2+}-APs by 1.1 nA, resulting in a coupling of 1.1 nA/1.7 nA = 65%. Voltages were measured at the positions indicated by triangles in *B*; red: dendritic recording/current injection; black: somatic recording/current injection. *B*: same as *A* but showing membrane potential in the entire dendritic tree. Voltages are color coded as indicated in the *top left*. The position of current injection is indicated by the red (dendritic) and white (somatic) arrowhead. At the time of AP initiation (*top*, 4.6 ms after the beginning of the somatic current injection), depolarization due to the bAP has already spread into the apical dendrite (in the case of bAP and BAC firing). *Bottom*: after 21 ms, the voltage deflection due to the bAP decayed back to baseline. Note that the spread of depolarization is almost the same for a dendritically elicited Ca^{2+}-AP and BAC firing. A movie can be found on our server (http://sun0.mpimf-heidelberg.mpg.de/~schaefer/BACFiring) and is also available as Supplementary Material at the *Journal of Neurophysiology* web site.

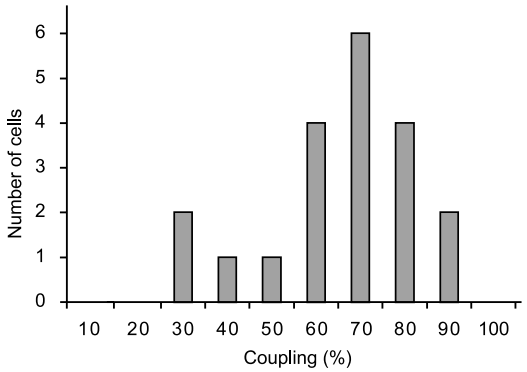

FIG. 3. Distribution of simulated BAC firing threshold reduction in reconstructed model neurons. The same distribution of channel densities and kinetics was implemented in 29 reconstructed cells. Of these, 21 cells were regularly spiking in response to simulated brief (5 ms) somatic current injection; 8 cells were intrinsically bursting. When simulated somatic and dendritic current injection were paired, 20 of the regularly spiking cells showed BAC firing with a BAC firing threshold reduction (coupling) of 69 ± 17%.

Starting with a cylinder (L = 1,000 μm), the morphology of the synthetic neuron under construction was modified by adding and removing branches to minimize the squared difference between the actual connectivity and the target connectivity. This process was repeated 300 times, and further repetition did not improve the connectivity match. The full implementation of the algorithm can be found at http://sun0.mpimf-heidelberg.mpg.de/~schaefer/BACFiring. For every section of dendrite between two branch points, a diameter was drawn from the distribution of diameter functions $D(x, y)$, according to its distance from the soma and the "end." Finally, the apical and basal dendrites were joined to a soma, and the entire synthetic neuron was scaled to its final size. Both final size and the length and diameter of the soma were again drawn from the respective distributions obtained from the reconstructed model neurons. Simulations were performed with this population of synthetic cells using the same passive and active membrane model as for the reconstructed cells (population 3; Fig. 5*G*).

SIMPLIFIED MODEL NEURONS (POPULATION 5). Simplified neurons were a third population of model neurons. They were generated as follows. The morphology of simplified neurons consisted of a soma (length, L = 80 μm; diameter, d = 45 μm; its size was increased to account for basal dendrite membrane area), three trunk segments (proximal: L = 90 μm, d = 7.5 μm; middle: L = 260 μm, d = 6 μm; distal: L = 290 μm, d = 5.5 μm), two tuft sections, both connected to the distal trunk (L = 400 μm, d = 7 μm), and two oblique dendrites (L = 200 μm, diameter varying as described) joined to the trunk at 90 and 350 μm distance from the soma, respectively. Passive membrane parameters and the active membrane model were the same as for the reconstructed (population 3) and synthetic (population 4) neurons (Fig. 7).

Active membrane model

The active membrane model is a set of instructions for the simulation program NEURON where (in the axon, soma, or dendrites) to place which types of channels at which density, using which gating kinetics. Active conductances were based on a previous model (Mainen and Sejnowski 1996) in which channels were distributed homogeneously in the dendrites. The following changes to this model were made to account for BAC firing: an active region (length: 100 μm; centered on the main bifurcation of the apical dendrite) with increased Ca^{2+} channel densities was introduced. The resulting variability in the distance of this region from the soma was not correlated with the variability in the simulated degree of coupling ($r = -0.24$, $P > 0.25$). The time constant for Ca^{2+} extrusion was decreased to τ_R = 80 ms; the exponent of the Ca^{2+} sensitivity of the Ca^{2+}-dependent K^+ channel was increased to caix = 4; its maximal activation and inactivation rate were increased to 0.05 and 0.1 ms^{-1}, respectively. The active membrane model also included a recently described A-type K^+ channel (Migliore et al. 1999). To account for the critical frequency effect (Larkum et al. 1999a), it was necessary to introduce a low threshold T-type Ca^{2+} current, $I_{caT} = g \times m^2h(v - E_{Ca})$, in the region around the main bifurcation with local channel density g = 5 pS/μm^2, activation m, and inactivation variable h. The membrane potential is given by v, and the reversal potential by E_{Ca}. The activation and inactivation variables were expressed in terms of a steady-state value m_∞ (v) and a time constant $\tau_m(v)$. The specific

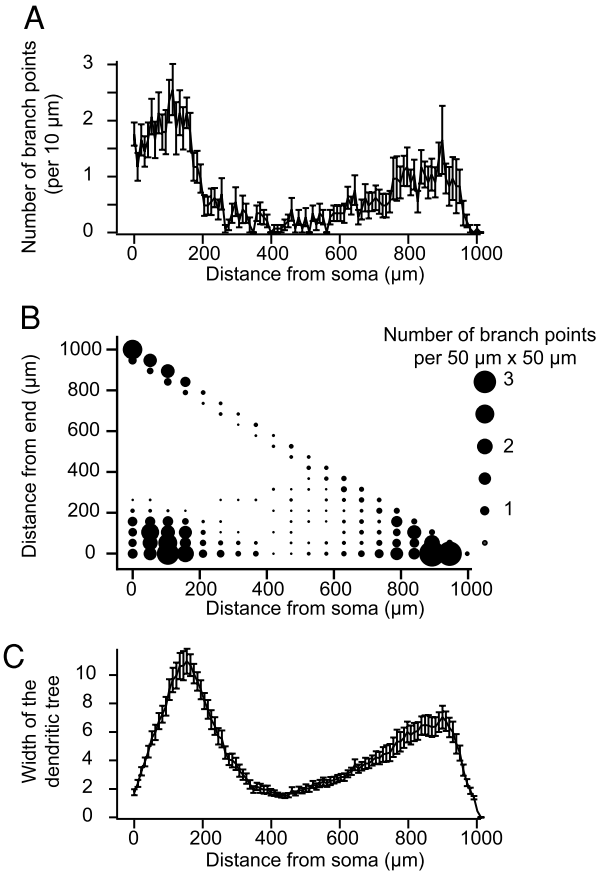

FIG. 4. Dendritic fingerprint determined for the apical dendrites of reconstructed L5 pyramidal neurons. *A*: 1-dimensional branch point density $B_1(x)$ for the apical dendrite as a function of the distance x from the soma. $B_1(x)$ is defined as the number of branch points per 10 μm dendritic length. *B*: 2-dimensional branch point density $B_2(x, y)$, calculated as the number of branch points with a distance x from the soma and y from the "end." Density is represented by point diameter as indicated by the scale on the *right*. Three regions can be identified. Data points in the *bottom left* correspond to branches of the oblique dendrites (small distance both from the soma and the end of the daughter branch). Region in *bottom right* can be identified as the population of tuft branches. Branch points are far away from the soma with varying but small distance from the end. Points on the diagonal represent branch points of the apical trunk and the longest branch in the tuft. Sum of the distances from soma and end is constant. *C*: width of the dendritic tree $W(x)$. $W(x)$ is calculated as the number of apical dendritic branches intersecting with a distance level x from the soma. Spatial resolution of the function $W(x)$ was 10 μm. Cells were normalized to 1,000 μm length of the apical dendrite. All parameters displayed were averaged across the ensemble of 29 reconstructed L5 pyramidal cells (in *A* and *B*, mean ± SE is shown). To complete the dendritic fingerprint, the same parameters were determined for the basal dendrites, as well as the diameter function $D(x, y)$, the number of basal dendrites, the length and diameter of the soma, and the maximal length before normalization of the cell size. This is outlined in detail in METHODS.

voltage dependencies were $m_\infty = 1/(1 + e^{-(v + 55\ mV)/7.4\ mV})$; $h_{inf} = 1/(1 + e^{(v + 75\ mV)/5\ mV})$; $\tau_m = 3\ ms + 1\ ms/(e^{(v + 60\ mV)/20\ mV} + e^{-(v + 135\ mV)/15\ mV})$; $\tau_h = 30\ ms + 1\ ms/(e^{(v + 66\ mV)/4\ mV} + e^{-(v + 425\ mV)/50\ mV})$. The channel distributions were modified from Mainen and Sejnowski (1996) as follows (in pS/μm^2): soma: $g_{Na} = 54$, $g_{Kv} = 600$, $g_{km} = 0.2$, $g_{K(Ca)} = 6.5$, $g_{Ka} = 600$, $g_{Ca} = 3$; dendrites: $g_{Na} = 27$, $g_{Kv} = 30$, $g_{Km} = 0.1$, $g_{K(Ca)} = 3.25$, $g_{Ka} = 300$, $g_{Ca} = 1.5$ In the active region, g_{Ca} was increased to 4.5.

Reconstructed axons were removed and replaced by an artificial axon (Mainen and Sejnowski 1996) to allow stable AP initiation. In the myelinated axon, C_m was reduced to 0.04 $\mu F/cm^2$, and R_m was reduced to 50 Ωcm^2 in the nodes of Ranvier. Channel densities were as follows: axon hillock and initial segment: $g_{Na} = 30{,}000$, $g_{Kv} = 3{,}000$; node of Ranvier: $g_{Na} = 30{,}000$; myelinated axon: $g_{Na} = 80$.

Degree of coupling

The degree of coupling is an empirical quantity calculated as the relative reduction (in %) of the threshold current (injected into the distal portion of the apical dendrite) that initiates a dendritic Ca^{2+}-AP when the dendritic current injection is preceded by a bAP

$$\text{degree of coupling} = (I_{Ca} - I_{BAC})/I_{Ca}$$

Here I_{Ca} and I_{BAC} are the smallest currents needed for evoking the Ca^{2+}-AP and BAC firing, respectively. This definition of the degree of coupling applies to experimental values and the values obtained from the simulations with reconstructed, synthetic, or simplified model neurons as described above. Other parameters characterizing coincidence detection are the optimal time and the width of the temporal window (Larkum et al. 1999b). Both are difficult to study experimentally with high precision. Analyzing the time window of coincidence detection in simulation yielded a half-width of 13.5 ± 1 ms (range, 11.4–14.1 ms), indicating that the contribution of morphological variation to variability in the width of the time interval is small.

Values are given as mean ± SD unless otherwise noted. Threshold was determined with an accuracy of 0.1 nA. In simulation, cells were defined as bursting if a brief (5 ms) somatic current injection evoked more than one AP at the current threshold. Dendritic current injected had the shape of a double exponential [$f(t) = (1 - e^{-t/\tau_1}) \times e^{-1/\tau_2}$] with $\tau_1 = 0.8$ ms and $\tau_2 = 4$ ms. The function was adjusted so that the peak current injection corresponded to the value referred to as the amplitude. The time constants were adjusted such that the dendritic potential measured at the distal pipette mimicked the compound excitatory postsynaptic potential (EPSP) in response to extracellularly evoked layer 1 input (Larkum et al. 1999b). The onset was 2–5 ms after the beginning of the somatic current pulse (Fig. 1*B*). As for bursting cells the somatic current injection alone evoked a long-lasting dendritic depolarization, these cells were fully coupled even without dendritic current injection. Therefore for the analysis of the simulations using reconstructed model neurons, bursting cells were excluded. Where this was not possible, because it would introduce a substantial selection bias (Fig. 5), a coupling value of 100% was assigned to the bursting cells.

Integral coupling

The integral coupling is defined as the time integral of the membrane depolarization ($\Delta V \times t$, given in mVms) measured at the position of the dendritic pipette during a bAP.

Dendritic fingerprint and distribution of dendritic fingerprints

The dendritic fingerprint refers to a set of eight quantities measured from the morphology of reconstructed neurons: *1*) one-dimensional branching density, *2*) two-dimensional branching density, *3*) the width of the dendritic tree, *4*) diameter distribution for the apical dendrite, *5*) diameter distribution for the basal dendrites, *6*) number of basal dendrites, *7*) somatic diameter and length, and *8*) maximal length of the nonnormalized apical dendrite from its origin on the soma to the most distal tip in the apical tuft.

These quantities were determined as follows: all distances and lengths in *1*)–*5*) and *8*) were measured along the dendrites in three dimensions. Neurons were normalized to a maximal dendritic length of 1000 μm; diameters were not scaled. *1*) The *one-dimensional branch point density* $B_1(x)$ was measured as the number of branch points per 10 μm as a function of the distance from the soma (example in Fig. 4*A*). *2*) The *two-dimensional branch point density* $B_2(x, y)$ was measured as the number of branch points with a distance x from the soma and y from the "end" (example in Fig. 4*B*). Here, "end" refers to the most distal tip of a daughter branch. Spatial resolution was 50 μm for both variables. *3*) The *width* of the dendritic tree $W(x)$ was measured as the number of branches that intersected with a distance level x from the soma. Spatial resolution of the function $W(x)$ was 10 μm (Fig. 4*C*). *4*) The *diameter function* $D(x, y)$ was measured as the average diameter of a branch with a distance x from the soma and y from the "end." *5*) These four parameter sets were also determined for the basal dendrites. *6*) The number of basal dendrites, as well as the *7*) diameter and length of the soma and *8*) the original maximal length of the apical dendrite were measured from the Neurolucida file.

RESULTS

BAC firing threshold reduction varies between individual cells

Dual whole cell recordings were made from the soma and distal apical dendrite of 37 thick tufted L5 pyramidal neurons (Fig. 1). The coupling between the proximal and the distal AP initiation zones was quantified as the relative decrease (in %) of the threshold current for evoking a Ca^{2+}-AP when preceded by a bAP. On average the degree of coupling in pyramidal neurons was 49 ± 17% (SD; range, 19–83%; $n = 37$). For 28 pyramidal neurons, the apical dendrite was reconstructed from the soma to the major bifurcation to ascertain the branching structure of the oblique dendrites.

Model of channel distributions and kinetics reproduces BAC firing in reconstructed model neurons

To isolate the contribution of differences in dendritic arborization between individual neurons to the variability in coupling, we first constructed model neurons ("reconstructed model neurons") with a standard channel density distribution and kinetics (referred to as the "active membrane model"), based on previous modeling studies (Mainen and Sejnowski 1996; Mainen et al. 1995). To simulate BAC firing in reconstructed neurons (Fig. 2), it was necessary to increase the density of Ca^{2+} channels in the proximity of the main bifurcation relative to the channel densities in the soma and the rest of the dendritic tree, as suggested previously (Elaagouby and Yuste 1999; Yuste et al. 1994). The properties of the active membrane were constrained by the requirement to qualitatively reproduce BAC firing when it was implemented in each of 29 morphological reconstructions of L5 pyramidal neurons. Thus the model was robust with respect to BAC firing and was not dependent on a specific L5 pyramidal cell morphology.

Variability of coupling with constant channel parameters

In simulations made with these 29 reconstructed neurons equipped with the active membrane model, 8 neurons gener-

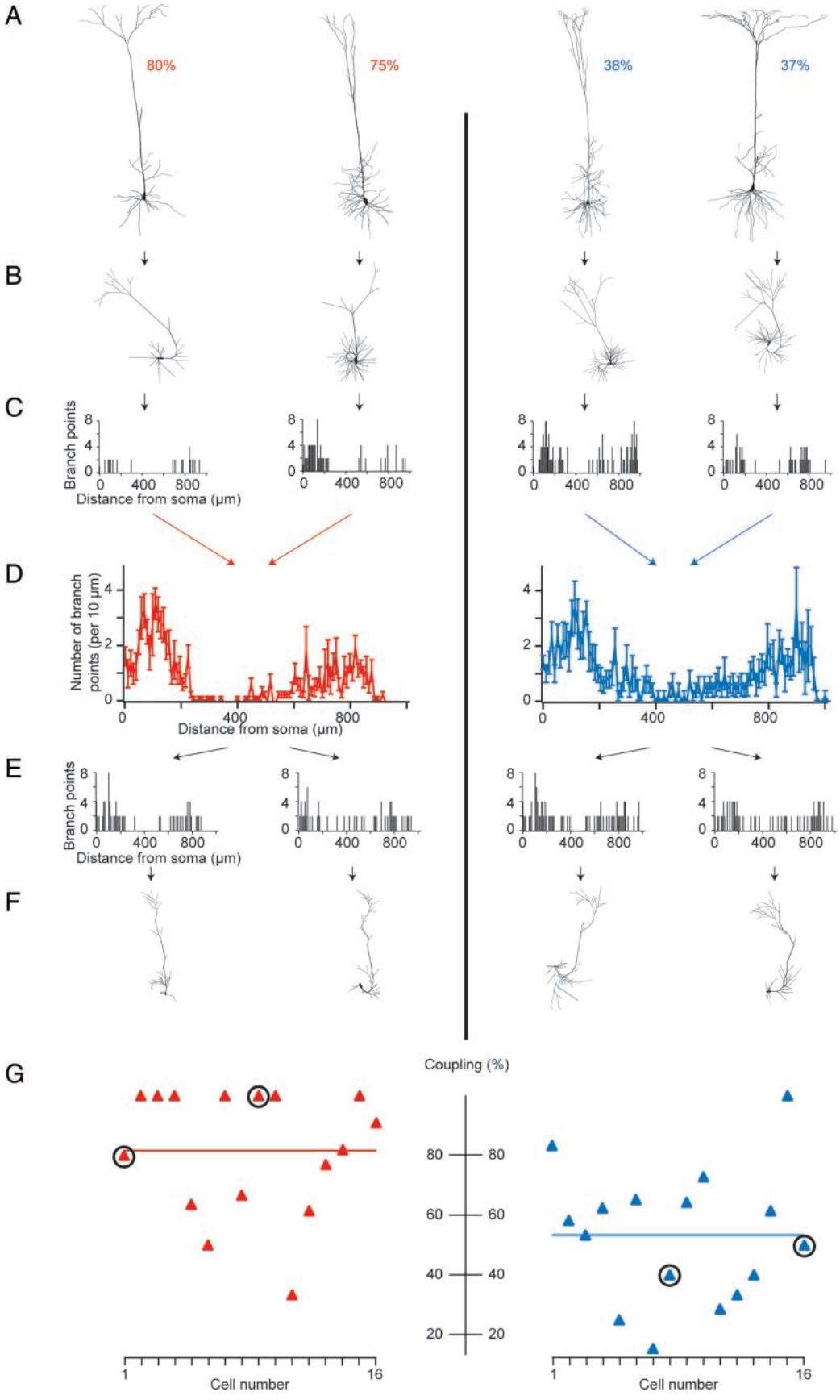
A
80%
75%
38%
37%
B
C
Branch points
Distance from soma (μm)
D
Number of branch points (per 10 μm)
Distance from soma (μm)
E
Branch points
Distance from soma (μm)
F
G
Coupling (%)
Cell number
Cell number

ated bursts of APs in response to brief current injection at the soma and were therefore not used to study coupling. The remaining 21 cells exhibited regular spiking behavior with simulated somatic current injection. Twenty of these showed BAC firing with a mean coupling of 69% (Fig. 3) and a variability (SD = 17%; range, 37–93%) similar to that observed experimentally. As channel distributions and kinetics were the same across cells, this variability can be attributed to differences in the dendritic morphology of the reconstructed cells.

Dendritic fingerprint captures variability of simulated coupling

The dependence on dendritic arborization in simulations suggests that it should be possible to extract geometric parameters that contribute to this variability. We therefore first quantified simple morphological properties of somata and dendrites for the 29 reconstructed neurons (Table 1). However, no correlation between coupling and any of these simple parameters could be detected (Pearson correlation coefficient $|r| < 0.32$).

As none of the simple geometric parameters captured the variation in dendritic arborization responsible for the variability in simulated coupling, we developed a more detailed dendritic fingerprint (Fig. 4) of L5 pyramidal neurons: it consisted of *1*) one- and *2*) two-dimensional branching densities, *3*) the width of the dendritic tree, and *4*) diameter distributions for the apical and *5*) basal dendrites, as well as *6*) the number of basal dendrites, *7*) somatic diameter and length, and *8*) the maximal length of the nonnormalized apical dendrite. These parameters are detailed in METHODS.

How do we know that this dendritic fingerprint is sufficiently complete to capture the contribution of morphology to the variability in (simulated) coupling (Fig. 3)? We divided the ensemble of reconstructed neurons into two groups according to their degree of coupling in the simulations: "strongly coupling cells" and "weakly coupling cells," respectively (Fig. 5*A*). We then calculated the dendritic fingerprint for all cells in each group, yielding distributions of the dendritic fingerprint for the two groups (Fig. 5*D*). Thirty-two "synthetic model neurons" were generated based on these distributions (Fig. 5, *E* and *F*), as described in METHODS.

The synthetic neurons allowed us to test whether the dendritic fingerprint was sufficient to capture possible morphological correlates of coupling: for each synthetic neuron, we implemented the same active membrane as described above for reconstructed neurons (Fig. 2) and simulated BAC firing. The average degree of coupling in the synthetic neurons was higher for those neurons generated from the parameters of the strongly coupling cells than for parameters taken from the weakly coupling cells (82 ± 21% vs. 53 ± 22%, *t*-test, $P < 0.0005$, Fig. 5*G*). This difference in synthetic neurons is highly significant and is comparable to the difference in coupling of strongly and weakly coupling reconstructed neurons (81 ± 7% vs. 58 ± 15%). We conclude that at least parts of the anatomical characteristics of the dendrites underlying the variability in simulated coupling are captured by the dendritic fingerprint (Fig. 4). The same held true for variations in other functional properties, such as the current threshold for evoking a Ca^{2+}-AP, and the somatic AP frequency needed to evoke a dendritic Ca^{2+} spike ("critical frequency") (Larkum et al. 1999a; data not shown).

TABLE 1. *Morphological characteristics of dendrites of 29 reconstructed L5 pyramidal neurons (mean ± SD)*

Length (μm) of apical dendrite	1300 ± 180
Length (μm) of apical trunk	680 ± 130
Rall ratio*	
At main bifurcation	1.3 ± 0.3
At oblique branching (mean)	1.2 ± 0.2
Membrane area (μm^2) of trunk	6,300 ± 1,300
Tuft	7,000 ± 3,600
Oblique dendrites	5,200 ± 2,700
Apical dendrite	18,500 ± 5,800
Basal dendrites	4,200 ± 2,000
Trunk diameter (μm)	
Average	4.8 ± 0.9
Start	6.3 ± 1.2
End	4.1 ± 1.0
Number of oblique dendrites	10.0 ± 3.3
Number of basal dendrites	6.6 ± 1.7

* The Rall ratio is defined as $(d_1^{3/2} + d_2^{3/2})/d_p^{3/2}$. d_1 and d_2 are the diameters of the first and second daughter branches; d_p is the diameter of the parent branch.

Position of oblique dendrites determines simulated coupling

The most profound difference in the branching parameters of the strongly and weakly coupling cells was in the branching densities in the tuft (beyond 800 μm in normalized length units) and at the apical dendrite at distances between 200 and 400 μm (Fig. 6*A*). At this region, the more distal of the oblique dendrites branch off the apical trunk. Neither the width of the dendritic tree nor the number of branch points as a function of the distance to the soma and to the end showed additional

FIG. 5. Dendritic fingerprint captures the essence of the morphological correlates of simulated coupling in reconstructed model neurons. *A*: reconstructed neurons that show BAC firing in the simulation are sorted according to their coupling. For display purposes, only 4 of the 20 neurons are depicted. Coupling (in %) in simulation is given next to each neuron. *B*: wiggles and angles between branches do not influence the electrophysiological properties in simulation and are reset arbitrarily to allow comparison with the synthetic model neurons. *C*: individual dendritic fingerprints are calculated for each reconstruction. For clarity, only the density of branch points along the apical dendrite is shown. *D*: distributions of morphological parameters, representing the dendritic fingerprint, are obtained for the strongly (red) and weakly (blue) coupling neurons. Again, only the density of branch points along the apical dendrite is shown (mean ± SE). *E*: parameters for the synthetic model neurons are drawn randomly from these distributions, forming a target connectivity. *F*: synthetic neurons are constructed according to this target parameter set as described in the METHODS. *G*: active membrane model is inserted into the synthetic neurons to determine BAC firing threshold reduction. Coupling was 82 ± 21% (SD) for the cells synthesized from the morphological parameters of the strongly coupling group and 53 ± 22% for the weakly coupling group (*t*-test, $P < 0.0005$). To avoid selection bias, bursting cells (cells effectively showing BAC firing without dendritic current injection) were counted as "fully coupled" (BAC firing threshold reduction = 100%) thus limiting the difference between the 2 groups.

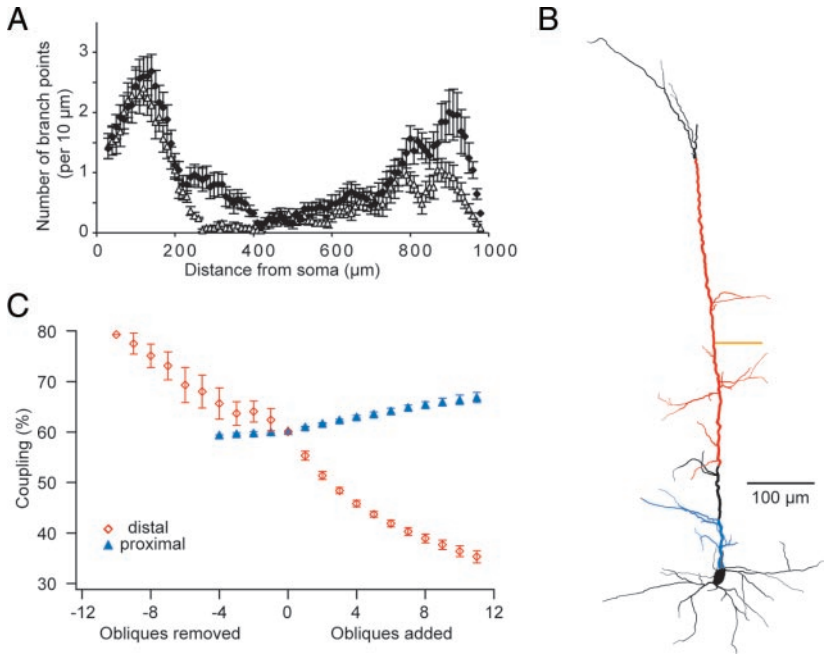

FIG. 6. Position of oblique dendrites influences simulated coupling in a reconstructed L5 pyramidal neuron. *A*: comparison of branching densities per 10 μm of apical dendrite of (in simulation) weakly (♦) and strongly (△) coupling reconstructed neurons (10 cells each, mean ± SE). For clarity, the graph was smoothed with a sliding window of 50 μm width. Distance is given as normalized distance. *B*: reconstruction of a L5 pyramid with highlighted proximal (blue, <100 μm from the middle of the soma) and distal (red, 200–700 μm) regions of the apical trunk used to study the location-dependent influence of oblique dendrites on coupling (C). "Proximal" and "distal" oblique dendrites are colored accordingly. An artificial oblique dendrite as added in *C* is depicted in orange (L = 70 μm, d = 3 μm). *C*: oblique dendrites were removed or artificial oblique dendrites (L = 70 μm; d = 3 μm, orange oblique dendrite in *B*) were added randomly with uniform probability per dendritic length at the 2 trunk regions shown in *B*. Active membrane model of channel density distributions and kinetics was inserted into the modified reconstructions and coupling was simulated. Coupling (in %) is shown for 20 trial morphologies each (mean ± SE). In *B* and *C*, distances are given in unnormalized coordinates.

pronounced differences. To further analyze the contribution of oblique dendrites, we first added simplified oblique dendrites (cylinders with L = 70 μm and d = 3 μm) to a reconstructed neuron in the distal region of the apical trunk (Fig. 6*B*, red). The simulated coupling decreased as expected (Fig. 6*C*). Neither the total membrane area of oblique dendrites nor the total number of oblique dendrites (Table 1) were correlated with the simulated degree of coupling. This indicates that the *position* where the oblique branches originate from the apical trunk might be the main factor determining coupling. We therefore added simplified oblique dendrites to a reconstructed neuron at more proximal locations (Fig. 6*B*, blue) and simulated BAC firing. The resulting coupling increased, while removal of oblique dendrites had the opposite effect (Fig. 6*C*). Closer examination of Fig. 6*A* reveals that oblique dendrites tend to decrease coupling if they are more distal than approximately 100–110 μm. Oblique dendrites increase coupling only if they are located closer than this roughly estimated "cutoff distance" (Fig. 6).

Simulated coupling in simplified model neurons

Why should the location of the oblique dendrites influence coupling? To answer this, we collapsed all proximal and all distal oblique dendrites into two oblique dendrites (Fig. 7*A*). A higher number of oblique dendrites in the reconstructed neurons was reflected in an increase in the diameter of the respective proximal or distal oblique dendrite in the simplified model

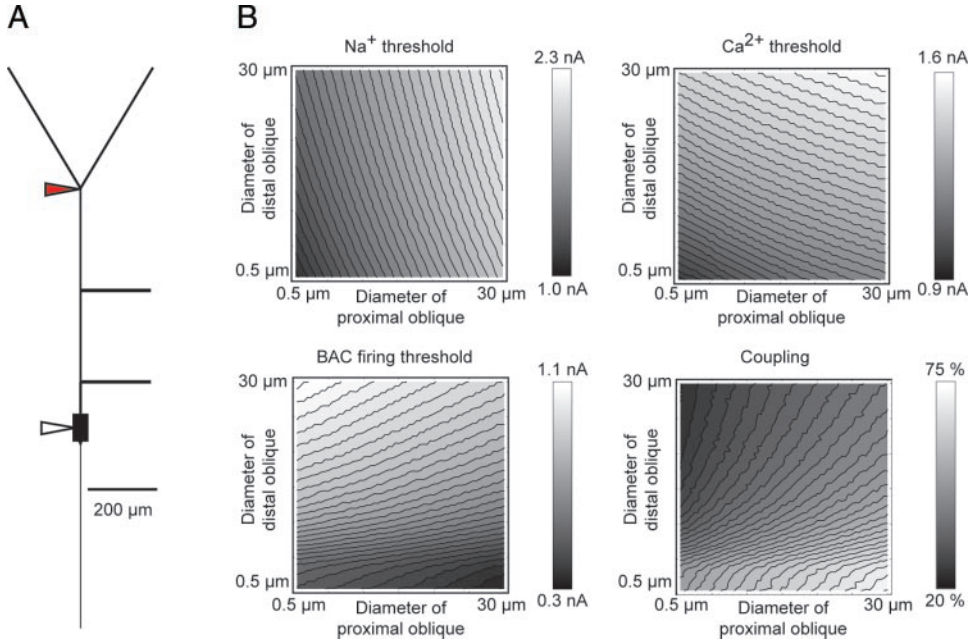

FIG. 7. Influence of proximal and distal oblique dendrites in a simplified model of L5 pyramidal neurons. *A*: morphology of the simplified model neuron that shows BAC firing. Arrowheads indicate point of current injection as in Fig. 2. Simplified morphology consisted of a soma (L = 80 μm, d = 45 μm), 3 trunk segments (proximal: L = 90 μm, d = 7.5 μm; middle: L = 260 μm, d = 6 μm, distal: L = 290 μm, d = 5.5 μm), 2 tuft sections (L = 400 μm, d = 7 μm), and 2 obliques (L = 200 μm, diameter varying as described in *B*) attached to the trunk at 90 and 350 μm distance from the soma. Axon and channel distributions are the same as in the simulations shown in Fig. 2. *B*: increasing the diameter of the distal oblique dendrite increases the current threshold for the Na^+-AP (*top left*), Ca^{2+}-AP (*top right*), and BAC firing (*bottom left*), and decreases coupling (*bottom right*). Increasing the diameter of the proximal oblique dendrite increases thresholds for the Ca^{2+}-AP and the Na^+-AP but decreases the BAC firing threshold and therefore increases coupling.

neuron. When the two diameters were varied simultaneously (Fig. 7*B*), we found that increasing the diameter of an oblique dendrite increased the current thresholds for both the Na^+- and the Ca^{2+}-AP. As expected, the oblique dendrite located closer to an initiation site influenced its current threshold more strongly. The Na^+-AP threshold was more sensitive to changes in the diameter of the proximal oblique than to changes in the diameter of the distal oblique, while the Ca^{2+}-AP threshold increased more steeply with increases in the diameter of the distal oblique dendrite. The coupling in simplified model neurons, however, increased with increasing diameters of proximal and decreasing diameters of distal oblique dendrites. This is consistent with the results from simulations using reconstructed model neurons (Fig. 6, *B* and *C*). The same results were obtained by replacing the active obliques with purely passive branchlets or even a simple shunt conductance at their origin in the apical dendrite (data not shown), indicating that the underlying mechanism did not depend on the details of the channel distribution or kinetics.

Variation of the diameters of the oblique dendrites resulted in a strong correlation between the degree of coupling and the time integral of the depolarization evoked by the bAP alone at the position of the dendritic pipette (referred to as the "integral coupling"; $r = 0.95$). The integral coupling can be studied also for active membrane models that are incapable of reproducing BAC firing. Thus we tested correlations between integral coupling and position of oblique dendrites for different models of the active membrane. Channel kinetics and distributions developed for models of *1*) L5 pyramidal cells (Mainen and Sejnowski 1996; Mainen et al. 1995), *2*) a CA1 pyramidal cell (Migliore et al. 1999), *3*) a thalamic relay neuron (Destexhe et al. 1998), as well as *4*) a passive model with only an active axon and soma but a completely passive dendritic tree were implemented in the simplified L5 pyramidal cell morphology (Fig. 7*A*). For all active and passive membrane models tested, increasing the diameter of distal obliques resulted in a decrease in the integral coupling, whereas an increase in the proximal oblique diameter enhanced the integral coupling (data not shown). This suggests that the influence of the dendritic branching pattern on BAC firing is largely insensitive to the underlying model of the active membrane.

Correlation between dendritic morphology and coupling in experiments

For 28 pyramidal cells whose BAC firing threshold reduction was measured in the experiment, the dendritic morphology could be recovered in sufficient detail to enable complete retrieval of the positions of all oblique dendrites. From the comparison of in simulation weakly and strongly coupling cells (Fig. 6*A*), a "cutoff distance" d was derived: Oblique dendrites located at the apical trunk more proximally than d improved coupling in simulation (Fig. 6). This distance was estimated to be 100–110 μm when the maximal length of the dendritic tree was normalized to 1,000 μm. This corresponds to approximately 140 μm in unnormalized coordinates (Table 1). Thus in the following, oblique dendrites closer than $d = 140$ μm are considered proximal. Comparison of the experimentally determined degree of coupling and the fraction of proximal obliques yielded a strong correlation ($r = 0.63$, $P < 0.0005$, Fig. 8).

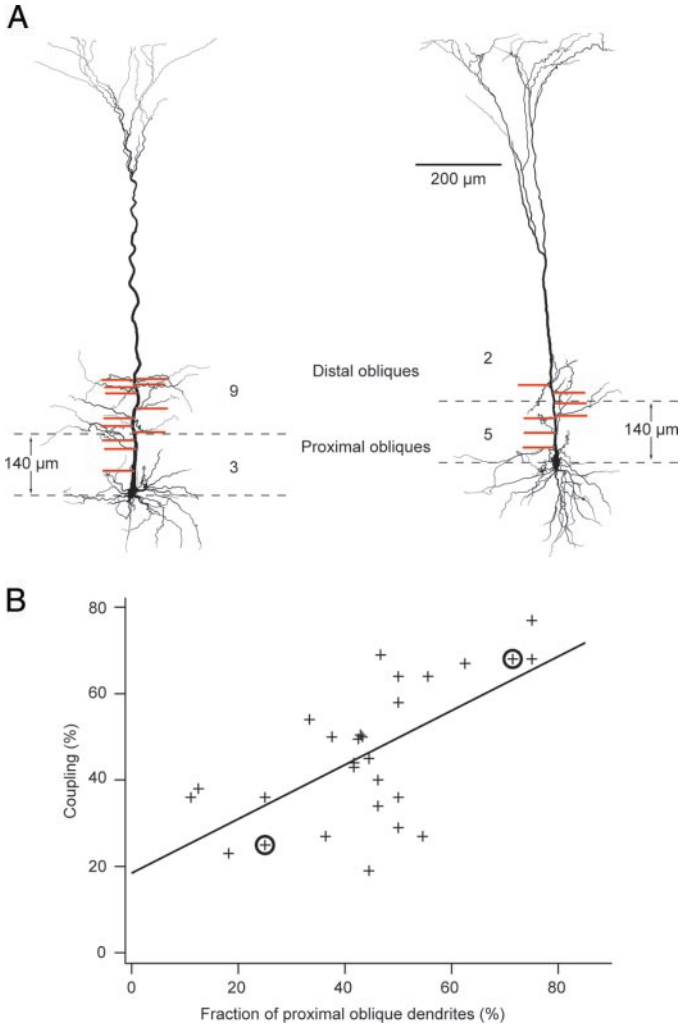

FIG. 8. Coupling is strongly correlated with position of oblique dendrites in the experiment. *A*: reconstruction of 2 L5 pyramidal neurons with experimentally measured coupling of 25% (*left*) and 68% (*right*). Positions of oblique dendrites are indicated by red bars. For the left neuron, 3 oblique dendrites branch off the apical trunk <140 μm away from the middle of the soma. As 9 oblique dendrites were located more distally, the fraction of proximal oblique dendrites was 3/12 = 25%. The fraction of proximal oblique dendrites for the right neuron was 5/7 = 71%. *B*: for 28 L5 pyramids, for which BAC firing threshold reduction was experimentally measured, the distances of oblique dendrites from the soma were determined in the light microscope as illustrated in *A*. Coupling increases with increasing fraction of oblique dendrites found within 140 μm distance from the soma ($r = 0.63$, $P < 0.0005$). Circles indicate the neurons from *A*. In all neurons, the oblique dendrites were unequivocally distinguishable from basal dendrites, as the soma-apical dendrite transition was clearly marked by a rapid change in diameter (maximal curvature) and no putative oblique dendrite was found within 5 μm of this transition. In addition, all reconstructions were performed ignorant to the experimentally measured coupling.

Consistent with the theoretical prediction (Figs. 6 and 7), enhanced coupling was associated with an increase in the number of proximal and a decrease in the number of distal oblique dendrites. Pyramids with a 10% larger fraction of proximal oblique dendrites ($d < 140$ μm) had, on average, a coupling that was 6.2% stronger. If the cutoff distance was changed between 70 and 210 μm, the correlation between coupling and the fraction of proximal oblique dendrites was still statistically significant (Fig. 9). However, the maximum

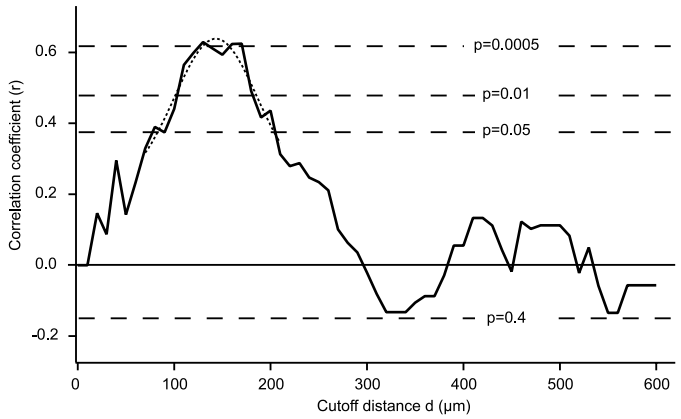

FIG. 9. Correlation between coupling and percentage of proximal oblique dendrites is largely independent of the cutoff distance. Positions of oblique dendrites were measured for the same 28 neurons as in Fig. 8*B*. The fraction $f(d)$ of oblique dendrites emerging from the apical trunk at distances less than a cutoff distance d was determined. The correlation $r(d)$ between experimentally measured coupling and $f(d)$ is plotted as a function of the cutoff distance d. Dashed lines indicate significance levels of the correlation. A Gaussian is fitted to $r(d)$ for cutoff distances that yield a significant correlation ($P < 0.05$). The peak of the Gaussian was at $d = 143$ μm. This essentially held true if distances were normalized to the apical trunk length or if the difference between the number of proximal and distal oblique dendrites rather than the fraction of proximal oblique dendrites was correlated with coupling ($r > 0.5$; maximum correlations between 130 and 170 μm from the soma).

correlation was reached at a cutoff distance of 143 μm, in agreement with the theoretical prediction.

DISCUSSION

Here we describe the influence of variation in dendritic morphology on the coupling between inputs arriving at different cortical layers (BAC firing, Larkum et al. 1999b). In simulations, we isolated differences in dendritic arborization as the only variable (Mainen and Sejnowski 1996) and determined the distribution of oblique dendrites as a correlate of coupling. A causal relationship between the position and number of dendrites and coupling was established by adding and removing branches and studying the resulting changes in the coupling of the reconstructed model neurons. This effect was not masked by other sources of variability, as also in the experiment coupling was highly correlated to the fraction of proximal oblique dendrites. Thus dendritic arborization is a determining factor for coupling in L5 pyramids in vitro. Recently, however, dendritic voltage transients similar to those evoked during BAC firing were observed in vivo (Larkum and Zhu 2002). There is also evidence for the occurrence of both dendritic Ca^{2+}-APs coupled to somatic activity and somatic spikes that do not elicit a dendritic Ca^{2+}-AP (Helmchen et al. 1999). In L2/3 pyramidal cells, backpropagating action potentials can be directly observed in vivo and their spread is very similar to the in vitro situation (Waters et al. 2001). It seems therefore likely that BAC firing occurs in vivo and is indeed variable.

Recent studies have proposed regulating mechanisms to "correct dendritic distortions," thus rendering synaptic input location-independent (Magee and Cook 2000). Other studies focus on putative heterogeneity in channel properties to explain variability in AP propagation (Golding et al. 2001). In this study, by combining simulations and experiments, we establish a causal relation between differences in dendritic arborization and the coupling between somatic and dendritic AP initiation sites within one class of cells, L5 pyramidal neurons. This relation prevails over putative compensatory mechanisms and is not outweighed by the cell-to-cell variability of voltage-gated channel properties and densities (Cook and Johnston 1997, 1999; Desai et al. 1999; Goldman et al. 2001). It is likely that variations in channel properties or densities also influence coupling. These contributions, however, would be either small and thus unable to mask the effect of differences in dendritic arborization (Fig. 8), or linked to the branching pattern such that they synergistically amplify the differences in coupling due to variation in dendritic arborization. To distinguish between these two alternatives would require a direct measurement of the cell-to-cell variability in the properties of several channel types simultaneously which is still impossible to perform.

Choice of experimentally tested morphological parameters

In comparison to other studies (Golding et al. 2001; Kim and Connors 1993; Vetter et al. 2001), we focused on an anatomical parameter that can be measured simply and reliably, the number and position of oblique dendrites. In general, it is difficult to determine dendritic diameters and thus dendritic membrane areas with sufficient accuracy at the LM level. In contrast, the branching pattern can be reliably measured. We observed that in simulation strong couplers had fewer oblique dendrites in the distal apical trunk and also fewer branches in the tuft. However, the number of oblique dendritic origins could be more reliably extracted from a biocytin-filled neuron than the branching density in the tuft region. In addition it was less likely to be influenced by damage caused by slicing.

Active membrane model

To study BAC firing in model neurons, a channel distribution was developed based on a published model (Mainen and Sejnowski 1996). In the model, BAC firing required an increase of Ca^{2+} channel densities in a region of the apical dendrite near the main bifurcation, consistent with experimental suggestions (Elaagouby and Yuste 1999; Helmchen et al. 1999; Schiller et al. 1995, 1997; Yuste et al. 1994) and other theoretical studies (M. London and I. Segev, personal communication). This assumption could be tested experimentally by determining Ca^{2+} channel densities along the apical dendrite, as has been done, e.g., for K^+, Na^+ and Ca^{2+} channels in hippocampal (Hoffman et al. 1997; Magee and Johnston 1995) and for Na^+ and K^+ channels in neocortical pyramidal cells (Bekkers 2000; Korngreen and Sakmann 2000; Stuart and Sakmann 1994).

In simplified model neurons we found a strong correlation between the degree of coupling and the time integral of the dendritic depolarization caused by the bAP. The dependence of this integral coupling on dendritic arborization was the same regardless of the underlying active membrane model. This suggests that the influence of oblique dendrites on coupling is robust to alterations of channel distributions and not an artifact of the active membrane model used.

Validation of the dendritic fingerprint using synthetic neurons

Previously synthetic neurons were mostly constructed to mimic the development of dendritic arborization (Ascoli et al. 2001; Van Ooyen et al. 1995). Here, we used synthetic neurons to validate the choice of morphological parameters comprising the dendritic fingerprint. We found that synthetic neurons derived from the fingerprint of strongly coupling reconstructed neurons indeed showed strong coupling in simulation, and neurons synthesized from the fingerprint of weak couplers showed weak coupling. As the neurons were synthesized based solely on the dendritic fingerprints, we conclude that *1*) the fingerprint captured those morphological properties that are relevant for the variability in coupling and *2*) the algorithm for synthesizing neurons is capable of conserving these differences. The dendritic fingerprint together with the algorithm to synthesize dendritic branching patterns could help in future studies to determine putative morphological correlates of other physiological properties, such as voltage-dependent amplification of EPSPs, efficacy of AP backpropagation, or various thresholds for initiation of dendritic Na^+, Ca^{2+}, or *N*-methyl-D-aspartate (NMDA) spikes.

Possible mechanisms underlying the influence of oblique dendrites on coupling

We suggest that two main mechanisms contribute to the effect of the branching pattern of the apical dendrite in influencing coupling. *1*) Additional branches increase the capacitive load for the bAP (a current sink). This effect becomes more prominent for distal dendrites as they are more remote from the large axosomatic current source that generates the AP. Concomitantly, proximal obliques are precharged by the somatic current injection. *2*) Additional proximal oblique dendrites increase the current threshold for evoking the somatic AP. The extra charge in the proximal oblique dendrites is then turned into a current source for the dendritic AP. It broadens the somatic AP, thus increasing coupling. Broader APs have also been implicated in facilitating backpropagation in CA1 pyramidal neurons (Golding et al. 2001); however, in our simulations, this is an effect entirely due to dendritic geometry. Solely increasing the diameter of proximal oblique dendrites increased the half-width of the somatic action potential in simulations in which all channel properties were kept constant. This effect was the less prominent the more distal the oblique dendrite was located and vanished beyond approximately 150 -200 μm (unpublished observation).

Functional implications

It is likely that other effects, such as neuromodulators (M. E. Larkum and B. Colmers, unpublished observations) or patterned inhibitory or excitatory input (Larkum et al. 1999b), also influence coupling. Since these modulations are transient, they would occur around a more slowly changing baseline determined by dendritic arborization. In general, slow modifications of the branching pattern are presumably controlled by local diffusible factors such as neurotrophins (Baker and van Pelt 1997; Baker et al. 1998; Horch and Katz 2002; Scott and Luo 2001) and by the detailed pattern of excitation and inhibition in proximity to the cell (Cline 2001; Maletic-Savatic et al. 1999).

The data presented here strongly suggest that this variation of dendritic arborization is a feature that tunes coincidence detection in pyramidal cells. This provides a mechanism by which structural plasticity (Poirazi and Mel 2001) can change the rules for dendritic integration of multilayer synaptic input to neocortical cells.

We thank Drs. Rainer Friedrich, Michael Häusser, Fritjof Helmchen, Katharina Kaiser, Alon Korngreen, Hugh Robinson, and Jack Waters for critical reading of the manuscript, Dr. Julius Zhu and A. Schmitt for providing some of the reconstructions, and Dr. Klaus Rohm and K. Bauer for expertly maintaining the computer environment.

REFERENCES

Ascoli GA, Krichmar JL, Nasuto SJ, and Senft SL. Generation, description and storage of dendritic morphology data. *Philos Trans R Soc Lond B Biol Sci* 356: 1131–1145, 2001.

Baker RE, Dijkhuizen PA, van Pelt J, and Verhaagen J. Growth of pyramidal, but not non-pyramidal, dendrites in long-term organotypic explants of neonatal rat neocortex chronically exposed to neurotrophin-3. *Eur J Neurosci* 10: 1037–1044, 1998.

Baker RE and van Pelt J. Cocultured, but not isolated, cortical explants display normal dendritic development: a long-term quantitative study. *Brain Res Dev Brain Res* 98: 21–29, 1997.

Bekkers JM. Distribution and activation of voltage-gated potassium channels in cell-attached and outside-out patches from large layer 5 cortical pyramidal neurons of the rat. *J Physiol* 525: 611–620, 2000.

Cline HT. Dendritic arbor development and synaptogenesis. *Curr Opin Neurobiol* 11: 118–126, 2001.

Connors BW and Gutnick MJ. Intrinsic firing patterns of diverse neocortical neurons. *Trends Neurosci* 13: 99–104, 1990.

Cook EP and Johnston D. Active dendrites reduce location-dependent variability of synaptic input trains. *J Neurophysiol* 78: 2116–2128, 1997.

Cook EP and Johnston D. Voltage-dependent properties of dendrites that eliminate location-dependent variability of synaptic input. *J Neurophysiol* 81: 535–543, 1999.

Desai NS, Rutherford LC, and Turrigiano GG. Plasticity in the intrinsic excitability of cortical pyramidal neurons. *Nat Neurosci* 2: 515–520, 1999.

Destexhe A, Neubig M, Ulrich D, and Huguenard J. Dendritic low-threshold calcium currents in thalamic relay cells. *J Neurosci* 18: 3574–3588, 1998.

Elaagouby A and Yuste R. Role of calcium electrogenesis in apical dendrites: generation of intrinsic oscillations by an axial current. *J Comput Neurosci* 7: 41–53, 1999.

Golding NL, Kath WL, and Spruston N. Dichotomy of action-potential backpropagation in CA1 pyramidal neuron dendrites. *J Neurophysiol* 86: 2998–3010, 2001.

Goldman MS, Golowasch J, Marder E, and Abbott LF. Global structure, robustness, and modulation of neuronal models. *J Neurosci* 21: 5229–5238, 2001.

Gupta A, Wang Y, and Markram H. Organizing principles for a diversity of GABAergic interneurons and synapses in the neocortex. *Science* 287: 273–278, 2000.

Häusser M, Spruston N, and Stuart GJ. Diversity and dynamics of dendritic signaling. *Science* 290: 739–744, 2000.

Helmchen F, Svoboda K, Denk W, and Tank DW. In vivo dendritic calcium dynamics in deep-layer cortical pyramidal neurons. *Nat Neurosci* 2: 989–996, 1999.

Hines ML and Carnevale NT. The NEURON simulation environment. *Neural Comput* 9: 1179–1209, 1997.

Hoffman DA, Magee JC, Colbert CM, and Johnston D. K^+ channel regulation of signal propagation in dendrites of hippocampal pyramidal neurons. *Nature* 387: 869–875, 1997.

Horch HW and Katz LC. BDNF release from single cells elicits local dendritic growth in nearby neurons. *Nat Neurosci* 5: 1177–1184, 2002.

Kim HG and Connors BW. Apical dendrites of the neocortex: correlation between sodium- and calcium-dependent spiking and pyramidal cell morphology. *J Neurosci* 13: 5301–5311, 1993.

Korngreen A and Sakmann B. Voltage-gated K^+ channels in layer 5 neocortical pyramidal neurones from young rats: subtypes and gradients. *J Physiol* 525: 621–639, 2000.

Larkum ME, Kaiser KMM, and Sakmann B. Calcium electrogenesis in distal apical dendrites of layer 5 pyramidal cells at a critical frequency of back-propagating action potentials. *Proc Natl Acad Sci USA* 96: 14600–14604, 1999a.

Larkum ME and Zhu JJ. Signaling of layer 1 and whisker-evoked Ca^{2+} and Na^{+} action potentials in distal and terminal dendrites of rat neocortical pyramidal neurons in vitro and in vivo. *J Neurosci* 22: 6991–7005, 2002.

Larkum ME, Zhu JJ, and Sakmann B. A new cellular mechanism for coupling inputs arriving at different cortical layers. *Nature* 398: 338–341, 1999b.

Larkum ME, Zhu JJ, and Sakmann B. Dendritic mechanisms underlying the coupling of the dendritic with the axonal action potential initiation zone of adult rat layer 5 pyramidal neurons. *J Physiol* 533: 447–466, 2001.

Magee JC and Cook EP. Somatic EPSP amplitude is independent of synapse location in hippocampal pyramidal neurons. *Nat Neurosci* 3: 895–903, 2000.

Magee JC and Johnston D. Characterization of single voltage-gated Na^{+} and Ca^{2+} channels in apical dendrites of rat CA1 pyramidal neurons. *J Physiol* 487: 67–90, 1995.

Mainen ZF, Joerges J, Huguenard JR, and Sejnowski TJ. A model of spike initiation in neocortical pyramidal neurons. *Neuron* 15: 1427–1439, 1995.

Mainen ZF and Sejnowski TJ. Influence of dendritic structure on firing pattern in model neocortical neurons. *Nature* 382: 363–366, 1996.

Major G, Larkman AU, Jonas P, Sakmann B, and Jack JJB. Detailed passive cable models of whole-cell recorded CA3 pyramidal neurons in rat hippocampal slices. *J Neurosci* 14: 4613–4638, 1994.

Maletic-Savatic M, Malinow R, and Svoboda K. Rapid dendritic morphogenesis in CA1 hippocampal dendrites induced by synaptic activity. *Science* 283: 1923–1927, 1999.

Migliore M, Hoffman DA, Magee JC, and Johnston D. Role of an A-type K^{+} conductance in the back-propagation of action potentials in the dendrites of hippocampal pyramidal neurons. *J Comput Neurosci* 7: 5–15, 1999.

Poirazi P and Mel BW. Impact of active dendrites and structural plasticity on the memory capacity of neural tissue. *Neuron* 29: 779–796, 2001.

Ramón y Cajal S. *Histology of the Nervous System of Man and Vertebrates.* New York: Oxford, 2001.

Roth A and Häusser M. Compartmental models of rat cerebellar Purkinje cells based on simultaneous somatic and dendritic patch-clamp recordings. *J Physiol* 535: 445–472, 2001.

Schiller J, Helmchen F, and Sakmann B. Spatial profile of dendritic calcium transients evoked by action potentials in rat neocortical pyramidal neurones. *J Physiol* 487: 583–600, 1995.

Schiller J, Schiller Y, Stuart G, and Sakmann B. Calcium action potentials restricted to distal apical dendrites of rat neocortical pyramidal neurons. *J Physiol* 505: 605–616, 1997.

Scott EK and Luo L. How do dendrites take their shape? *Nat Neurosci* 4: 359–365, 2001.

Segev I, Rinzel J, and Shepherd GM. *The Theoretical Foundation of Dendritic Function.* Cambridge, MA: MIT Press, 1995.

Serodio P and Rudy B. Differential expression of Kv4 K^{+} channel subunits mediating subthreshold transient K^{+} (A-type) currents in rat brain. *J Neurophysiol* 79: 1081–1091, 1998.

Stuart GJ and Sakmann B. Active propagation of somatic action potentials into neocortical pyramidal cell dendrites. *Nature* 367: 69–72, 1994.

Talley EM, Cribbs LL, Lee JH, Daud A, Perez-Reyes E, and Bayliss DA. Differential distribution of three members of a gene family encoding low voltage-activated (T-type) calcium channels. *J Neurosci* 19: 1895–1911, 1999.

Van Ooyen A, van Pelt J, and Corner MA. Implications of activity dependent neurite outgrowth for neuronal morphology and network development. *J Theor Biol* 172: 63–82, 1995.

Vetter P, Roth A, and Häusser M. Propagation of action potentials in dendrites depends on dendritic morphology. *J Neurophysiol* 85: 926–937, 2001.

Waters J, Larkum ME, Sakmann B, and Helmchen F. Active dendritic properties of rat neocortical layer 2/3 pyramidal neurons. *Soc Neurosci Abstr* 27: 502.8, 2001.

Yuste R, Gutnick MJ, Saar D, Delaney KR, and Tank DW. Ca^{2+} accumulations in dendrites of neocortical pyramidal neurons: an apical band and evidence for two functional compartments. *Neuron* 13: 23–43, 1994.